Progress In Electromagnetics Research C, Vol. 89, 111–120, 2019

Bandwidth Enhancement of Wideband Dual-Polarized Antenna with Loaded Open Stubs for Wireless Communication

Zhaoyang Tang* and Yingzeng Yin

Abstract—In this paper, a wideband ±45° dual-polarized antenna is proposed for the wireless communication. An annular ring patch with four arc-shaped slots is employed to generate a wide operating impedance bandwidth. By introducing four open stubs to the antenna element, the impedance bandwidth is enhanced. The antenna has a broad impedance bandwidth (VSWR < 2) of 51.2% (1.63–2.75 GHz) and a high port-to-port isolation of 27 dB over the entire band of operation. In addition, a 1 × 4 antenna array is developed for the wireless communication. Experimental results illustrate that the antenna array features wide operational bandwidth, high port isolation and superior radiation performance.

1. INTRODUCTION

Owing to the superior features of combating multipath fading effect and strengthening communication channel capacity [1], the antenna with polarization diversity is widely applied in the operating bands of 2G (1.71–1.92 GHz), 3G (1.88–2.17 GHz) and LTE (2.3–2.4 GHz and 2.5–2.69 GHz) communication systems. In addition, designing a broadband antenna can save installation space and reduce the cost of equipment. As a result, a broadband dual-polarized antenna with an operational band of 1.71–2.69 GHz plays an important role in the wireless communication systems.

Currently, piles of wideband dual-polarized antennas have been proposed in [2–13]. Cross dipole antennas in [2–5] and patch antennas in [6–8] are two classic wideband antenna types. In the design of [9], a dual-polarized antenna with wide operating band, high port isolation and good radiation performances is proposed by loading some dipoles. Nevertheless, it is difficult to massively assemble due to the 3-D structure. Combining electric dipoles and magnetic dipoles, a new dual-polarized antenna type (called as a magneto-electric dipole antenna) is proposed [10]. The antenna has a wide impedance bandwidth (VSWR < 2) of 23% (1.71–2.17 GHz) and a port isolation higher than 28 dB, and the heavier weight is a significant drawback because of the metal structure. Slot antenna is another antenna type [11–13]. In [13], combining dual resonant modes of a stepped slot resonator, a wide bandwidth (return loss > 10 dB) of 31.2% (1.68–2.3 GHz) is obtained at two ports. Obviously, its operating band does not meet the requirement of 1.71–2.69 GHz.

In this paper, a wideband dual-polarized antenna is presented for wireless communication. Owing to the loaded open stubs, the operating impedance bandwidth is significantly enhanced for the antenna element. Based on the proposed antenna element, a 1×4 antenna array is designed, fabricated and tested. Measured results demonstrate that both antenna element and antenna array feature wide operating band, high port isolation, stable gains as well as stable radiation pattern for dual polarizations. Detailed discussions about the antenna element and antenna array are shown as follows.

Received 23 November 2018, Accepted 14 December 2018, Scheduled 27 December 2018

* Corresponding author: Zhaoyang Tang (zhaoyangt@126.com).

The authors are with the National Key Laboratory of Antennas and Microwave Technology, Xidian University, Xi'an, Shaanxi 710071, China.

2. DUAL-POLARIZED ANTENNA ELEMENT

2.1. Antenna Configuration

The configuration of the proposed dual-polarized antenna element is displayed in Figure 1. The proposed antenna consists of an annular ring patch with arc-shaped slots, open stubs, coplanar striplines, two Y-shaped feeding lines, two 50-Ω coaxial cables, two metal pins and a square ground plane. The annular ring patch is printed on the bottom side of an FR4 substrate ($\varepsilon_r = 4.4$, $\tan\delta = 0.02$, and thickness = 0.8 mm) while Y-shaped feeding lines are etched on the top side of the same substrate. To avoid overlap between the feeding lines, partial part of one feeding line is shifted to the bottom layer of the substrate, and two metal vias are utilized to connect the bottom and top parts of the feeding line. Two ports (designated as port 1 and port 2) are used to excite the antenna through coaxial cables, as shown in Figure 1(c). The inner conductor of each coaxial cable is connected to the feeding line whereas its outer conductor is soldered on the ring patch. As can be seen, the antenna is slant $+45°$ polarization when port 1 is excited. Similarly, a slant $-45°$ polarization is realized when port 2 is driven. Two metal pins between the ring patch and ground plane are utilized to work as baluns for balance-to-unbalance transformer. The antenna element is supported by four plastic posts and fixed above a square ground plane to implement a unidirectional radiation. With the help of soft Ansys HFSS v.16, the design dimensions are listed as follows: $R = 21.4$ mm, $H = 26$ mm, $Hs = 0.8$ mm, $a1 = 68$ degree, $Lg = 140$ mm, $Ld = 65$ mm, $L1 = 14.2$ mm, $L2 = 7$ mm, $L3 = 5.1$ mm, $L4 = 6$ mm, $L5 = 2.4$ mm, $Wa = 1.5$ mm, $Wr = 8.6$ mm, $Wt = 0.9$ mm, $Ws = 1$ mm, $W1 = 0.9$ mm, $W2 = 1$ mm, $W3 = 1.8$ mm, $W4 = 1.3$ mm.

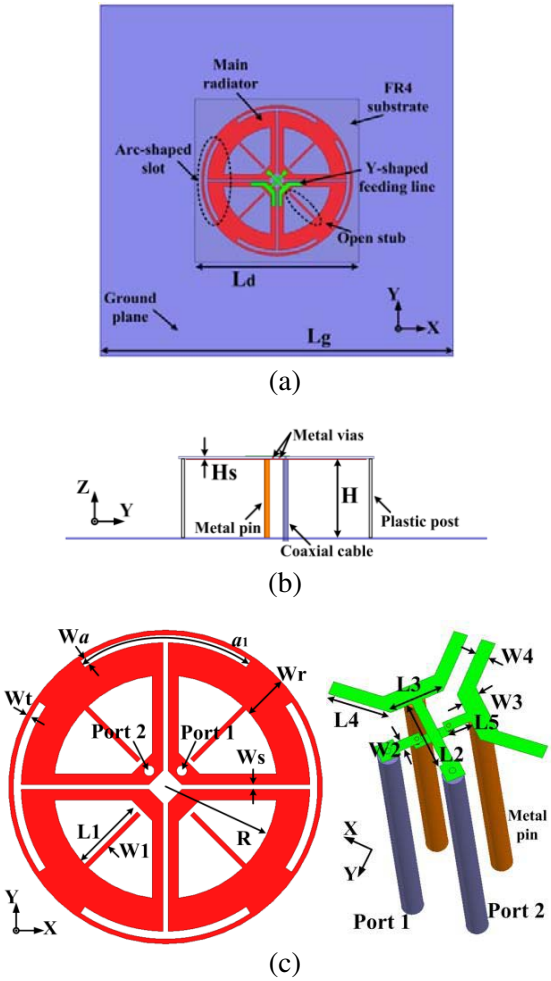

Figure 1. Configuration of the dual-polarized antenna: (a) top view, (b) side view, (c) detailed view.

2.2. Design Analysis

A comparison of the simulated impedance bandwidths with and without open stubs is depicted in Figure 2 to explain the principle for the bandwidth enhancement. It is observed that a wide operating band with dual resonant frequencies is gained without open stubs. However, a new resonant mode is induced at 2.8 GHz after loading the open stubs. Combining three resonant modes, a wide impedance bandwidth is realized for the antenna element.

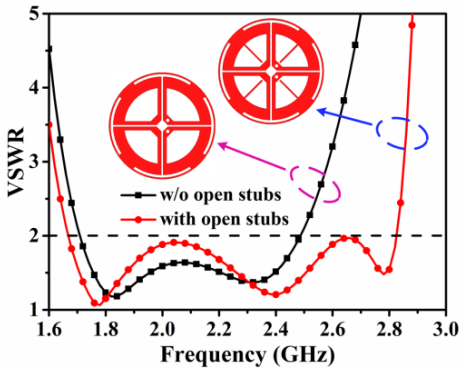

Figure 2. Simulated VSWRs of the antenna with and without open stubs.

Figure 3 shows the current distributions of the antenna at different operating frequencies when port 1 is driven. At 1.8 GHz, the current is mainly concentrated on the outer edge of the ring patch and coplanar striplines, which means that the ring patch determines the resonant modes at lower frequency band. At high frequency of 2.8 GHz, the current is strongly induced on the inner edge of the ring patch, open stubs, and coplanar striplines. In this case, a new resonant mode is induced because open stubs are adopted.

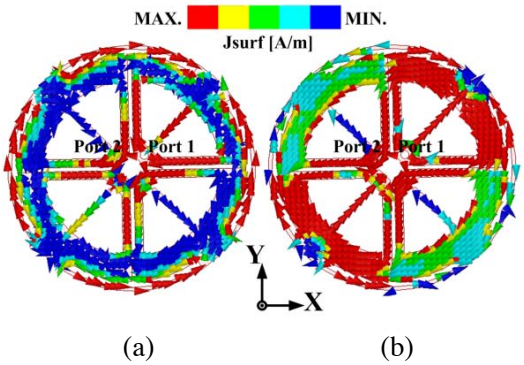

Figure 3. Current distributions of the antenna as port 1 is excited at (a) 1.8 GHz and (b) 2.8 GHz.

To investigate the design parameters' effect on the impedance bandwidth of the antenna, key parameters, including the width Wr of the ring patch, length L_1 of the open stub, angle a_1 of the arc-shaped slot, and height H of the radiator, are studied.

Figure 4 shows the effect of parameter Wr on the VSWR. It can be seen that two resonant frequencies in the low and middle frequency bands move toward the low frequency band as Wr increases. This is because the current path length determining the resonant mode is lengthened. We also see that Wr has a little effect on the resonant mode at high frequency. Moreover, the curves rise in the high frequency band as Wr increases, which indicates that parameter Wr affects the impedance matching at high frequency. Finally, $Wr = 8.6$ mm is selected to realize a wide operating band.

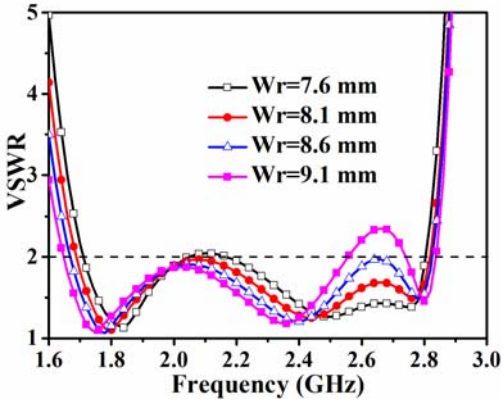

Figure 4. Simulated VSWRs versus parameter Wr.

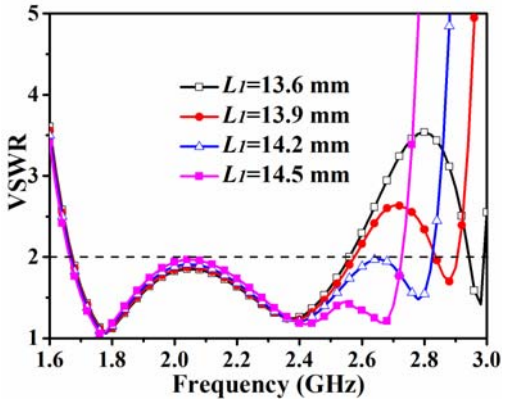

Figure 5. Simulated VSWRs versus parameter L_1.

Figure 5 shows the effect of parameter L_1 on the VSWR. It can be observed that the resonant frequency at high frequency gradually moves toward the low frequency band when L_1 increases. This is because parameter L_1 extends the physical length of the resonant mode. Moreover, it has a little effect on the other two resonant frequencies at low frequency band. At last, $L_1 = 14.2\,\text{mm}$ is selected for widening the impedance bandwidth.

Figure 6 shows the effect of parameter a_1 on the VSWR. We can see that parameter a_1 has a big effect on the impedance matching. The curves in the middle frequency band shift down gradually but rise in the high frequency band, which means that the impedance matching becomes better in the middle frequency band but worse in the high frequency band. Finally, $a_1 = 68$ degrees is chosen for obtaining a wide operating band with good impedance matching.

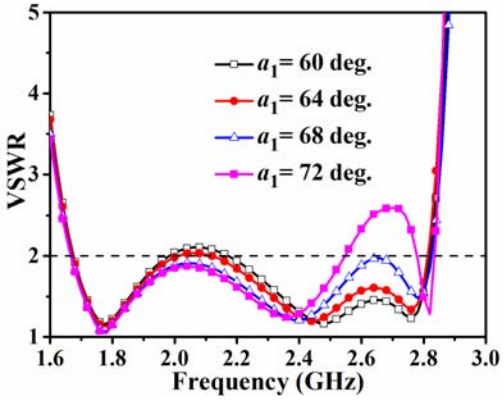

Figure 6. Simulated VSWRs versus parameter a_1.

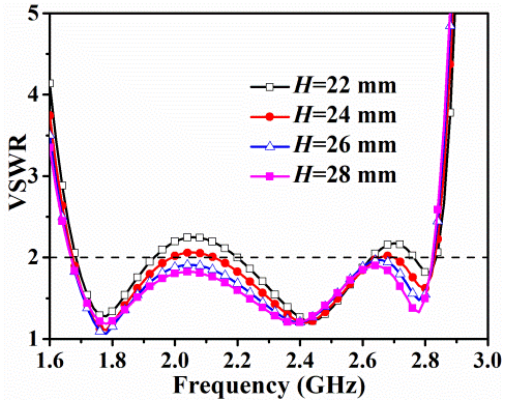

Figure 7. Simulated VSWRs versus parameter H.

Figure 7 shows the effect of parameter H on the VSWR. It can be seen that parameter H mainly affects the impedance matching of the antenna. The curves shift down gradually over the whole operational band as H increases, indicating that the impedance matching becomes better. Finally, $H = 26\,\text{mm}$ is chosen for improving impedance matching.

2.3. Experimental Results

A prototype of the antenna plotted in Figure 8 is fabricated and tested. The simulated and measured VSWRs and isolations are obtained, as shown in Figure 9. Owning to the accuracy of the network analyzer and fabrication tolerance, there is a little discrepancy between the simulated and measured

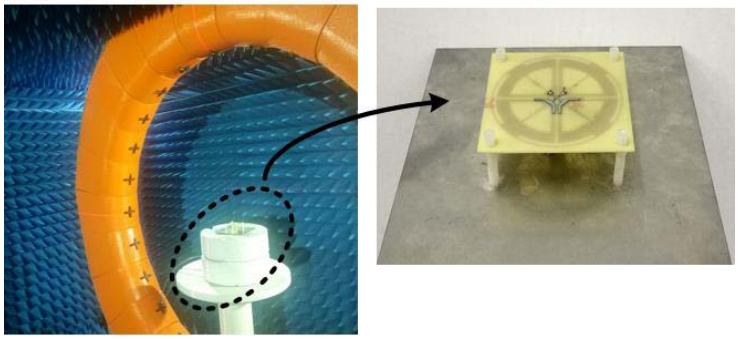

Figure 8. Proposed antenna prototype in the microwave anechoic chamber.

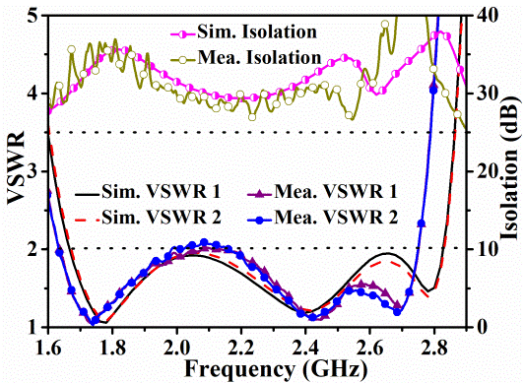

Figure 9. Simulated and measured VSWRs and isolations of the antenna element.

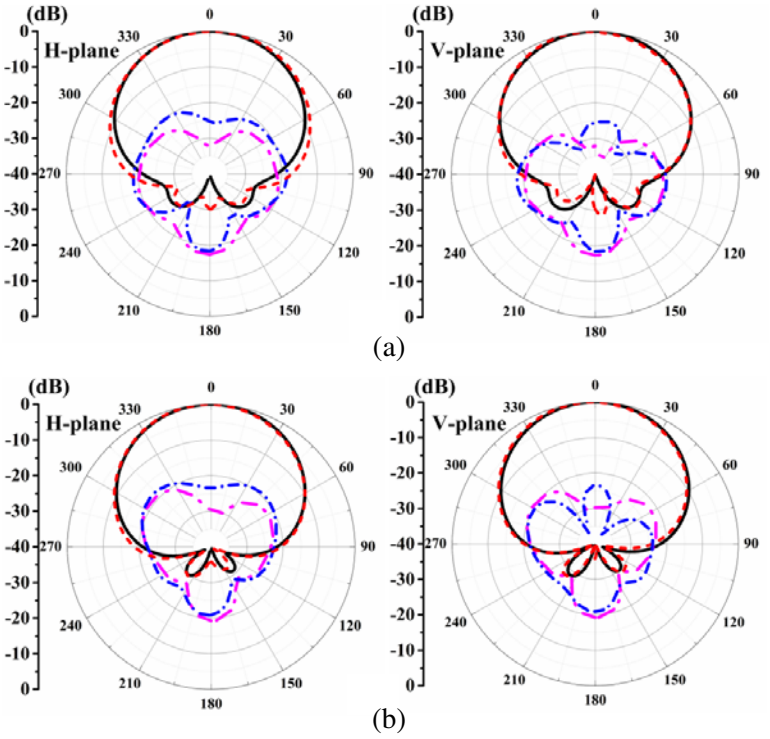

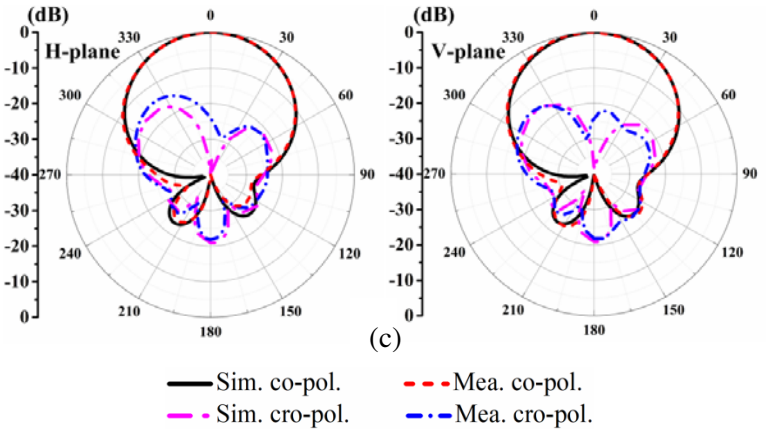

Figure 10. Radiation patterns of the antenna element as the port 1 is excited at (a) 1.7 GHz, (b) 2.2 GHz, and (c) 2.7 GHz.

results. Measured results illustrate that the antenna has a broad impedance bandwidth (VSWR < 2) of 51.2% (1.63–2.75 GHz). Moreover, the measured port isolation is higher than 27 dB over the entire band of operation.

Figure 10 shows the simulated and measured radiation patterns of the antenna element. According to the position of the base-station antenna in practical application, we redefine xz- and yz-planes as the horizontal plane (H-plane) and vertical plane (V-plane), respectively. Here, we just give the radiation patterns of $+45^\circ$ polarization due to the symmetric configuration. It can be seen that a little difference occurs between the simulated and measured radiation patterns because of the testing environment and fabrication tolerance. In addition, the radiation pattern remains stable across the operating band, and the cross-polarization level is less than -24 dB at boresight. Meanwhile, the measured efficiency of the antenna is over 80% across the operating band.

Figure 11 shows the simulated and measured antenna gains and half-power beamwidths (HPBWs) in the H-plane. It can be observed that the measured gain around 8.1 ± 0.7 dBi and HPBWs around $61^\circ \pm 6.5^\circ$ are implemented within the entire operating band.

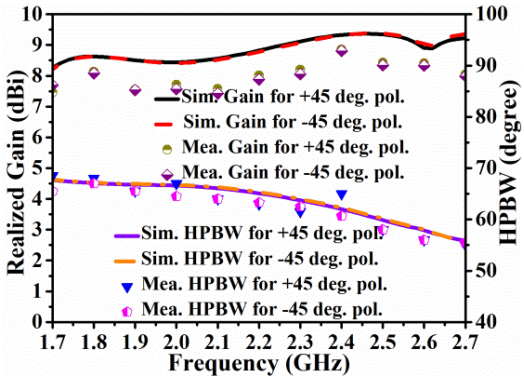

Figure 11. Simulated and measured gains and HPBWs of the antenna.

3. DUAL-POLARIZED ANTENNA ARRAY

3.1. Array Geometry

A 1×4 dual-polarized antenna array is designed to meet the requirements of higher gain and narrower beamwidth for base-station applications. The geometry of 1×4 antenna array is plotted in Figure 12(a).

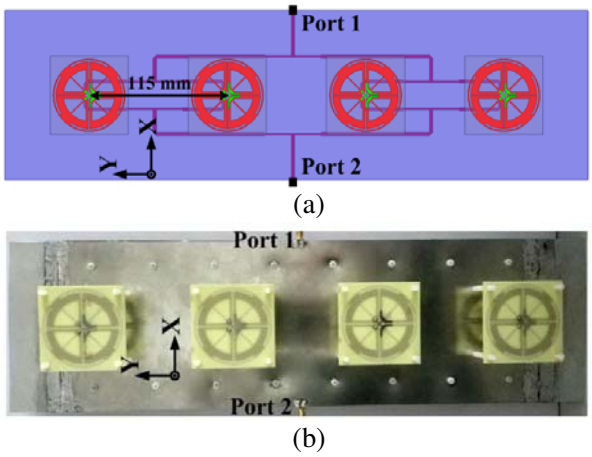

Figure 12. 1×4 antenna array: (a) geometry and (b) prototype.

The element spacing is 115 mm for obtaining a wide bandwidth and high gain. Two 4-way power dividers are adopted to excite the antenna array for realizing dual polarizations. Note that the power dividers are fabricated on a 1-mm-thick F4B substrate ($\varepsilon r = 2.65$, $\tan\delta = 0.002$). A prototype of 1×4 antenna array is plotted in Figure 12(b).

3.2. Experimental Results

Figure 13 shows the simulated and measured VSWRs and isolations of 1×4 antenna array. It is observed that a common -10-dB impedance bandwidth obtained is 48.1% (1.69–2.76 GHz) at two ports. In addition, the port isolation is better than 24 dB over the entire band of operation.

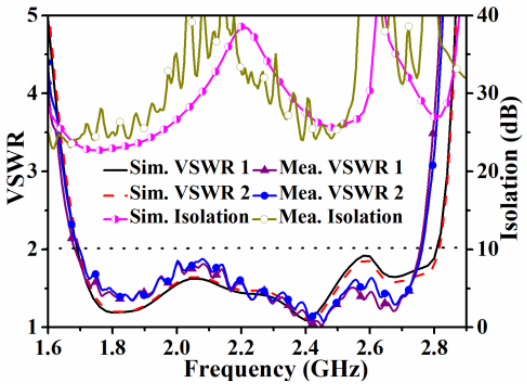

Figure 13. Simulated and measured VSWRs and isolations of the antenna array.

Figure 14 shows the simulated and measured radiation patterns of the antenna array. Owing to the symmetric configuration of the antenna array, we display only the radiation patterns of $+45°$ polarization. It can be seen that a stable radiation pattern is implemented across the entire operating band. The cross-polarization level at boresight is less than -17 dB.

Figure 15 displays the simulated and measured gains and HPBWs of the antenna array. It can be concluded that the measured antenna array gain is around 13 ± 1 dBi within the operational band. The measured HPBWs are around $63.5° \pm 4.5°$ in the H-plane for dual polarizations.

Table 1 lists a comparison between the proposed and reported antennas. The proposed antenna has a lower profile than those in [2, 4, 10, 12]. In addition, it has a wider impedance bandwidth than those in [2, 4, 8, 10, 13] and a higher port isolation than those in [8, 12]. We also see that the obtained

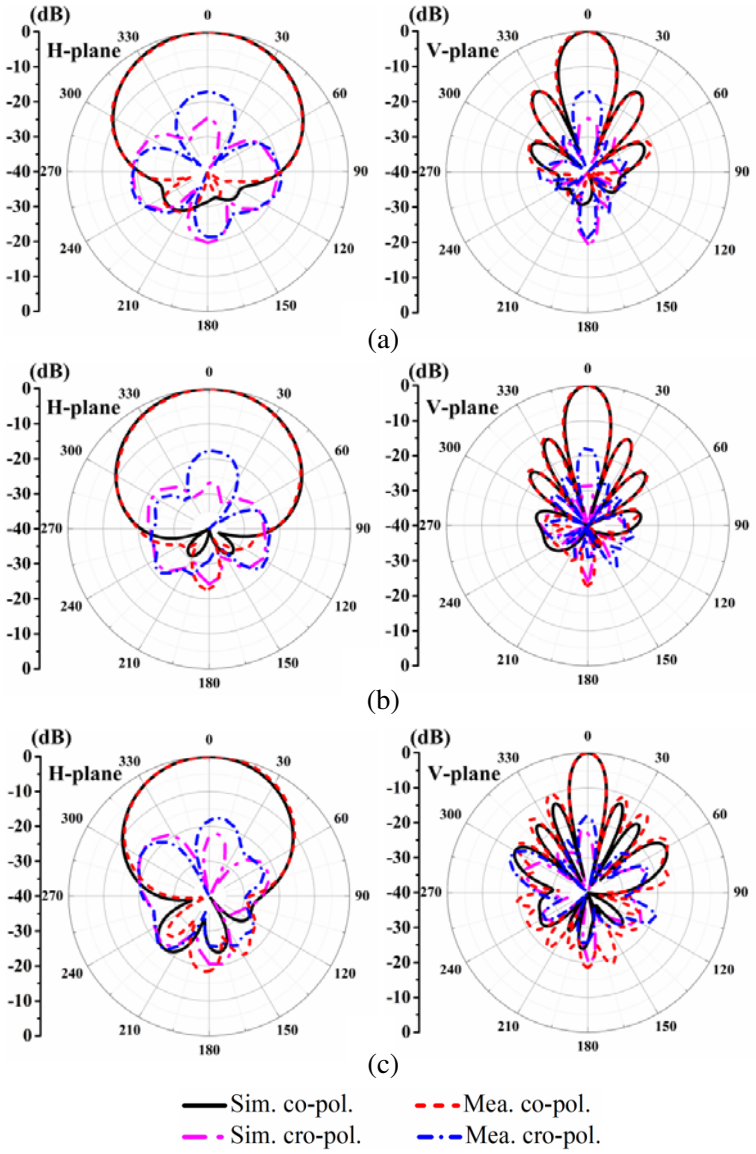

Figure 14. Radiation patterns of the antenna array as the port 1 is excited at (a) 1.7 GHz, (b) 2.2 GHz, and (c) 2.7 GHz.

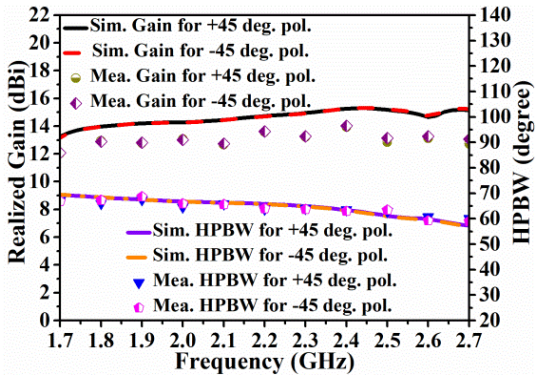

Figure 15. Simulated and measured gains and HPBWs of the antenna array.

Table 1. Comparison of the proposed and reported antennas.

References	Dimensions (λ_0^3)	Bandwidth (GHz)	Isolation (dB)	Gain (dBi)
[2]	$0.734 \times 0.734 \times 0.294$	1.71–2.69 (VSWR < 2)	31	> 7
[4]	$0.856 \times 1.317 \times 0.306$	1.63–2.32 ($\|S_{11}\| < -10$ dB)	32	8.6 ± 0.2
[8]	$0.992 \times 0.992 \times 0.109$	1.68–2.04 (VSWR < 2)	25	~ 10
[10]	$1.105 \times 1.105 \times 0.258$	1.71–2.17 ($\|S_{11}\| < -10$ dB)	28	~ 6.6
[12]	$0.965 \times 0.965 \times 0.257$	1.56–2.73 ($\|S_{11}\| < -10$ dB)	26	7.85 ± 0.75
[13]	$1.327 \times 1.327 \times 0.153$	1.68–2.3 ($\|S_{11}\| < -10$ dB)	30	NG
Pro.	$1.022 \times 1.022 \times 0.196$	1.63–2.75 (VSWR < 2)	27	8.1 ± 0.7

λ_0 represents the wavelength at center frequency of operation.
NG: not given.

antenna gain is higher than those in [2, 10, 12]. In a word, our work has a lower profile, wider operating band, higher port isolation, and higher gain.

4. CONCLUSION

A wideband dual-polarized antenna is presented in this paper. The operating impedance bandwidth of the antenna element is widened by loading additional four open stubs. Measured results show that the antenna has a broad impedance bandwidth of 51.2% (1.63–2.75 GHz) for VSWR < 2. Moreover, the port isolation is better than 27 dB and the cross-polarization level less than -24 dB over the entire operating band. A 1×4 antenna array is developed, fabricated, and tested. Based on the experimental results, it can be concluded that the antenna array features wide operating band, high port isolation, stable gains as well as stable radiation pattern for both polarizations. Finally, the proposed antenna element and antenna array are suitable for wireless communication applications.

REFERENCES

1. Wong, K. L., *Compact and Broadband Microstrip Antennas*, Wiley, Hoboken, NJ, USA, 2002.
2. Lee, H. and B. Lee, "Compact broadband dual-polarized antenna for indoor MIMO wireless communication systems," *IEEE Trans. Antennas and Propag.*, Vol. 64, No. 2, 766–770, 2016.
3. Cui, Y. H., R. L. Li, and H. Z. Fu, "A broadband dual-polarized planar antenna for 2G/3G/LTE base stations," *IEEE Trans. Antennas and Propag.*, Vol. 62, No. 9, 4836–4840, 2014.
4. Zuo, S. L., Q. Q. Liu, and Z. Y. Zhang, "Wideband dual-polarized crossed-dipole antenna with parasitical crossed-strip for base station applications," *Progress In Electromagnetics Research C*, Vol. 48, 159–166, 2014.
5. Xie, J. J. and Q. Song, "Wideband dual-polarized dipole antenna with differential feeds," *Progress In Electromagnetics Research Letters*, Vol. 59, 43–49, 2016.
6. Wang, Y. and Z. W. Du, "Dual-polarized slot-coupled microstrip antenna array with stable active element pattern," *IEEE Trans. Antennas and Propag.*, Vol. 63, No. 9, 4239–4244, 2015.
7. Mak, K. M., X. Gao, and H. W. Lai, "Low cost dual polarized base station element for long term evolution," *IEEE Trans. Antennas and Propag.*, Vol. 62, No. 11, 5861–5865, 2014.
8. Lai, H. W. and K. M. Luk, "Dual polarized patch antenna fed by meandering probes," *IEEE Trans. Antennas and Propag.*, Vol. 55, No. 9, 2625–2627, 2007.
9. Luo, Y. and Q. X. Chu, "Oriental crown-shaped differentially fed dual-polarized multidipole antenna," *IEEE Trans. Antennas and Propag.*, Vol. 63, No. 11, 4678–4685, 2015.
10. Mak, K. M., H. Wong, and K. M. Luk, "A shorted bowtie patch antenna with a cross dipole for dual polarization," *IEEE Antennas Wireless Propag. Lett.*, Vol. 12, 265–268, 2013.

11. Jiang, X. L., Z. J. Zhang, Z. J. Tian, Y. Li, and Z. H. Feng, "A low-cost dual-polarized array antenna etched on a single substrate," *IEEE Antennas Wireless Propag. Lett.*, Vol. 6, 126–129, 2007.
12. Zhou, C. F., H. Wong, and L. K. Yeung, "A wideband dual-polarized inductor-end slot antenna with stable beamwidth," *IEEE Antennas Wireless Propag. Lett.*, Vol. 17, No. 4, 608–612, 2018.
13. Lian, R. N., Z. D. Wang, Y. Z. Yin, J. J. Wu, and X. Y. Song, "Design of a low-profile dual-polarized stepped slot antenna array for base station," *IEEE Antennas Wireless Propag. Lett.*, Vol. 15, 362–365, 2016.